Mineralium Deposita (2004) 39: 159–172
DOI 10.1007/s00126-003-0389-5

ARTICLE

**Chusi Li · Zhanghua Xu · Sybrand A. de Waal**
**Edward M. Ripley · Wolfgang D. Maier**

# Compositional variations of olivine from the Jinchuan Ni–Cu sulfide deposit, western China: implications for ore genesis

Received: 25 April 2003 / Accepted: 31 August 2003 / Published online: 25 October 2003


**Abstract** The Jinchuan Ni–Cu sulfide deposit is hosted by an elongated, olivine-rich ultramafic body that is divided by subvertical strike-slip faults into three segments (central, eastern, and western). The central segment is characterized by concentric enrichments of cumulus olivine crystals and interstitial sulfides (pyrrhotite–pentlandite–chalcopyrite intergrowth), whereas the eastern and western segments are characterized by an increase of sulfides toward the lower contacts. In all segments sulfides are concentrated at the expense of intercumulus silicates. Olivine re-crystallization is found to be associated with actinolite alteration in some samples. The compositional variations of primary olivine from the sulfide-poor samples can be explained by a small degree of olivine crystallization ($< 5\%$) from a basaltic magma followed by local re-equilibration of the olivine with up to 30% trapped silicate liquid. In the sulfide-bearing samples the compositions of primary olivine record the results of olivine-sulfide Fe–Ni exchange that occurred after the trapped silicate liquid crystallized. Our olivine data indicate that Ni in the original sulfide liquids increased inward in the central segment and laterally away from the lower contact in the eastern segment. Variations in the compositions of sulfide liquids are thought to result from fractional segregation of immiscible sulfide liquid from a basaltic magma in a staging chamber instead of in situ differentiation. High concentrations of olivine crystals (mostly $> 50$ modal%) and sulfide (averaging $\sim 5$ wt%) in the rocks are consistent with the interpretation that the Jinchuan deposit was formed by olivine- and sulfide-laden magma successively ascending through a conduit to a higher, now-eroded, level. Sulfide enrichment toward the center in the central segment and toward the lower contact in the eastern and western segments may have, in part, resulted from flow differentiation and gravitational settling during magma ascent, respectively.

**Keywords** Jinchuan · Magma conduit · Ni · Olivine · Sulfide

Editorial handling: P. Lightfoot

C. Li (✉) · E. M. Ripley
Department of Geological Sciences,
Indiana University, Bloomington, IN 47401, USA
E-mail: cli@indiana.edu
Tel.: +1-812-8555404
Fax: +1-812-8557899

Z. Xu · S. A. de Waal · W. D. Maier
Centre for Research on Magmatic Ore Deposits,
Department of Earth Sciences, University of Pretoria,
Pretoria 0002, South Africa

## Introduction

Magmatic Ni–Cu sulfide ore deposits are hosted by komatiite lavas or variably differentiated intrusions with a basaltic bulk composition. The four largest komatiite-associated Ni-sulfide camps in the world are Thompson, Raglan, Kambalda, and Perseverance (Lesher and Keays 2002). Sudbury, Jinchuan, and Noril'sk represent the three largest Ni-sulfide camps in the world that are associated with broadly basaltic rocks (Naldrett 1998). Sudbury and Noril'sk are clusters of many deposits in variable sizes, whereas Jinchuan is a single super large deposit. The Sudbury deposits are believed to be of meteorite impact origin (Lightfoot et al. 2001). The Noril'sk deposits are related to sulfide accumulation in magma conduits in response to assimilation of country rock sulfur (Naldrett and Lightfoot 1999; Li et al. 2003a).

The Jinchuan ultramafic body was discovered in 1958 and the follow-up exploration proved that it hosts $> 400$ million tons of sulfide ores grading 1.2% Ni and 0.7% Cu (Chai and Naldrett 1992a). Since mining started in 1973, the Jinchuan mine has been the most important Ni producer in China. The remarkable and enigmatic feature about Jinchuan is that a vast accumulation of sulfide occurs in a small ultramafic body without immediate sulfur-rich country rocks.

Previous investigators of Jinchuan (Tang 1990, 1993; Tang and Li 1995) proposed that differentiation of ultramafic magma and immiscible sulfide liquids took place at depth within a stratified staging chamber in which sulfide liquids concentrated toward the bottom and silicate melt toward the top. The first magma extracted from the upper part of the staging chamber formed unmineralized intrusions. This was followed by removal of sulfide-bearing magma and sulfide liquids from the staging chamber to form the Jinchuan deposit. Chai and Naldrett (1992b) proposed an alternative model. They suggested that the Jinchuan body represents the root of a much larger layered intrusion of basaltic magma instead of ultramafic magma.

Olivine is the predominant cumulus mineral in the Jinchuan body. Its compositions can be directly related to parental magma compositions if a correction is made for the effects of interaction with trapped silicate and sulfide liquids and hydrothermal alteration. This paper reports the results of a detailed study of olivine compositional variations, which has significant implications for the genesis of sulfide mineralization in the Jinchuan body.

## Geological background

The geology of the Jinchuan Ni–Cu sulfide deposit and its host rocks has been described by Tang (1990, 1993), Tang and Li (1995), Chai and Naldrett (1992a, 1992b), and Zhou et al. (2002). The Jinchuan body is one of several mafic–ultramafic bodies located in an uplifted, northwest-striking terrain of Lower Proterozoic migmatites, gneisses and marbles that form a southeast-facing monoclinal sequence, overlain to the southwest by Upper Proterozoic conglomerates, sandstones, limestones, and schists (Fig. 1a). Tang et al. (1992) determined a Sm–Nd age of $1{,}508 \pm 31$ Ma for the intrusion. Immediate country rocks to the Jinchuan body are predominantly marbles with minor granitoids.

The Jinchuan body has been divided by a series of northeast-trending, subvertical strike-slip faults into several segments (Fig. 1b). Chai and Naldrett (1992a, 1992b) referred to these fault-bounded segments as subchambers. The present Jinchuan body is dyke-like in most places and sill-like in a limited area in the eastern segment (see cross sections of Tang and Li 1995). In the central segment, sulfides are concentrated toward the center. In the western and eastern segments, sulfides are concentrated toward the NW contact (Fig. 1b). A common feature in all segments is that disseminated and net-textured sulfide ore bodies occur parallel to the NW contact in most places. Discordant massive sulfide veins of a few meters long and tens of centimeters to more than 20 m thick that crosscut disseminated and net-textured sulfide ore bodies are also present, but only in limited places. Evidence of original intrusive contacts with country rocks such as chilled margins and textural gradations from contacts have been obscured in places by severe post-magmatic hydrothermal alteration and shear deformation. Metasomatic skarn and sulfide veins that originate from massive sulfide bodies occur in nearby marbles in some places.

De Waal et al. (2003) proposed that the sill-like part of the Jinchuan body represents a better preserved portion of an originally sill-like intrusion and the dyke-like parts are related to post-emplacement block rotation during the regional Longshoushan uplifting event.

## Sampling and analytical methods

A total of 120 samples were collected from three drill cores (I14–16, II14–83, and II48–136) located in three different segments. The locations of these cores are shown in Fig. 1b. Samples of quarter core of about 20 cm in length were collected at regular intervals (10–20 m) in each core.

Petrographic examination of the samples was conducted using a standard optical microscope, followed by detailed back-scattered electron imagery using a CAMECA SX50 electron microprobe at Indiana University. About two-thirds of the samples collected contain unaltered olivine crystals or olivine remnants in serpentine networks. The compositions of olivine were determined by wavelength dispersive analysis. An accelerating voltage of 15 kV was used with a beam current and counting time for major elements of 20 nA and 20 s, respectively. Nickel was analyzed using a beam current of 100 nA and a counting time of 100 s. The detection limit for Ni under these conditions was about 60 ppm. International oxide and silicate standards were used for calibration. The accuracy of olivine analysis was monitored using San Carlos Olivine (USNM 1113122/444) reference material. Sample reproducibility for Ni and forsterite (Fo) contents varied by less than 2%. The average compositions of 5–12 grains, and 3–5 spots per gain of primary olivine from each sample are listed in Table 1.

## Results

### Effect of alteration

The samples from this study may be broadly described as sulfide-poor and sulfide-bearing peridotites. They contain 40-80% medium- to coarse-grained cumulus olivine with minor cumulus orthopyroxene ($< 2\%$) and Cr-spinel ($< 3\%$) that are present as inclusions in olivine. Interstitial phases, in descending order of abundance, are orthopyroxene, plagioclase and clinopyroxene. Cumulus orthopyroxene distinguishes itself from intercumulus orthopyroxene by its low Al and Ca contents (De Waal et al. 2003). Cr-spinel crystals commonly contain ilmenite lamellae or rims. The compositions of the Cr-spinel are highly variable (Barnes and Tang 1999). Most samples are highly serpentinized and exhibit a characteristic net

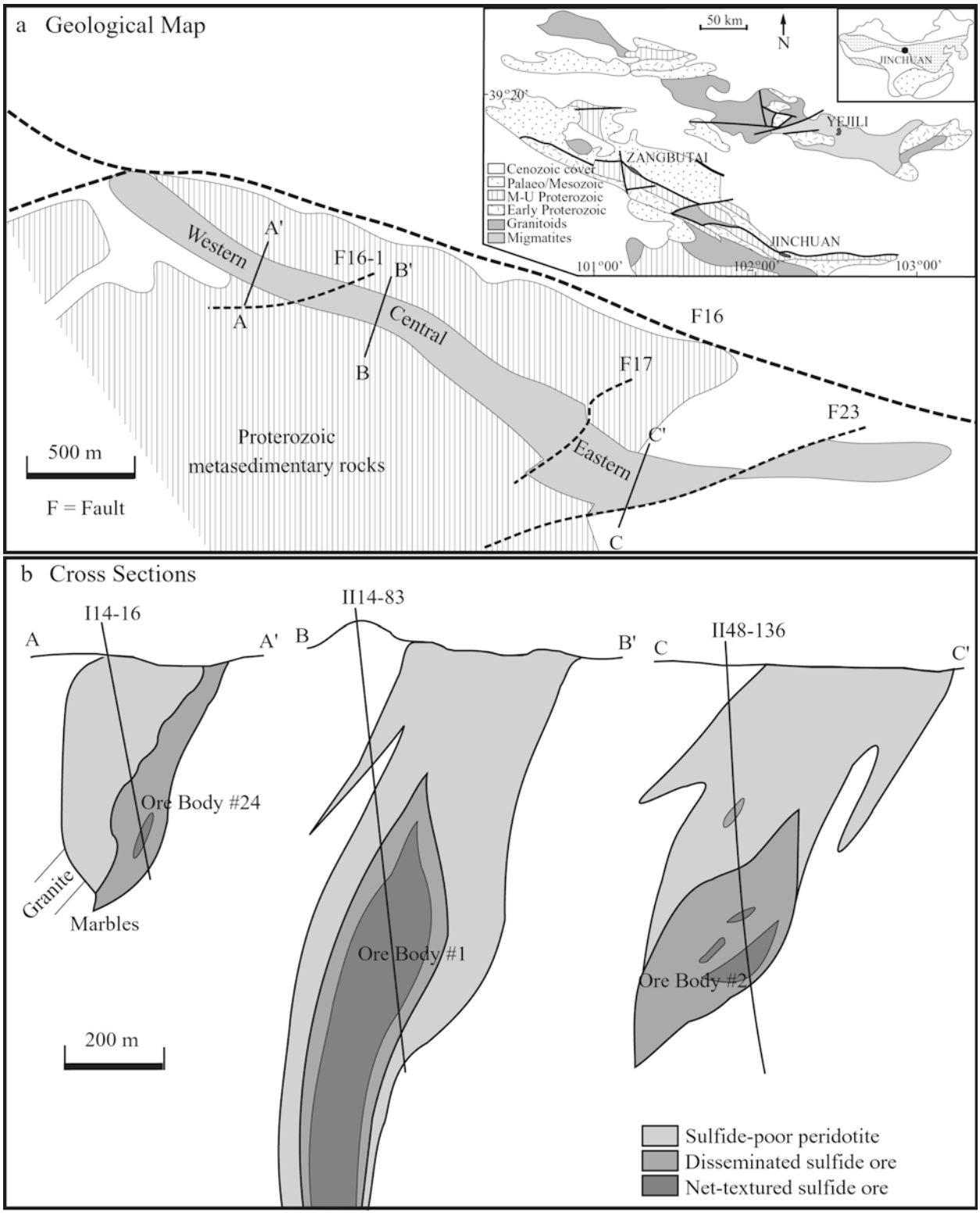


**Fig. 1** Geological map and cross sections of the Jinchuan deposit. There are more than five boreholes in each section, but only the ones we have sampled are shown

texture in which irregular remnant olivine kernels occur in a network of serpentine. Unaltered olivine crystals, mostly as inclusions in pyroxene, are found in less than 15% of the samples (Fig. 2a, b). In the samples with incipient alteration of pyroxene to Mg-hornblende and chlorite, the rim of coexisting olivine is recrystallized to form a more Fe-rich variant (Fig. 2b). With progress of alteration, tremolite appears in the place of Mg-hornblende, and the size of the recrystallized olivine rim

**Table 1** The compositions of olivine from the Jinchuan intrusion

| Sample no. | Depth | $SiO_2$ | $Cr_2O_3$ | MgO | CaO | MnO | FeO | NiO | Total | Fo | Ni |
|---|---|---|---|---|---|---|---|---|---|---|---|
| | | (wt%) | | | | | | | | (mol%) | (ppm) |
| Drill core I14-16 | | | | | | | | | | | |
| 31 | 77 | 39.67 | 0.01 | 42.83 | 0.06 | 0.22 | 16.39 | 0.22 | 99.40 | 82.20 | 1,695 |
| 30 | 85 | 39.65 | 0.03 | 43.42 | 0.07 | 0.23 | 16.50 | 0.22 | 100.12 | 82.30 | 1,692 |
| 29 | 98 | 39.42 | 0.01 | 43.85 | 0.06 | 0.22 | 16.09 | 0.22 | 99.86 | 82.81 | 1,692 |
| 28 | 106 | 39.27 | 0.02 | 44.08 | 0.06 | 0.21 | 16.37 | 0.23 | 100.23 | 82.64 | 1,778 |
| 26 | 124 | 40.17 | 0.01 | 45.31 | 0.10 | 0.19 | 13.88 | 0.23 | 99.89 | 85.27 | 1,798 |
| 25 | 133 | 39.91 | 0.01 | 44.97 | 0.12 | 0.19 | 14.20 | 0.23 | 99.63 | 84.92 | 1,782 |
| 24 | 143 | 40.07 | 0.02 | 44.98 | 0.13 | 0.20 | 14.10 | 0.23 | 99.73 | 85.03 | 1,789 |
| 23 | 153 | 40.05 | 0.02 | 44.62 | 0.11 | 0.23 | 14.60 | 0.23 | 99.86 | 84.42 | 1,799 |
| 21 | 165 | 39.76 | 0.02 | 44.40 | 0.07 | 0.20 | 15.16 | 0.23 | 99.85 | 83.84 | 1,798 |
| 20 | 175 | 39.82 | 0.01 | 44.06 | 0.11 | 0.20 | 15.29 | 0.23 | 99.72 | 83.65 | 1,814 |
| 18 | 209 | 39.88 | 0.02 | 44.62 | 0.06 | 0.23 | 14.63 | 0.24 | 99.68 | 84.33 | 1,848 |
| 17 | 220 | 39.47 | 0.01 | 43.86 | 0.09 | 0.24 | 16.36 | 0.21 | 100.26 | 82.59 | 1,679 |
| 16 | 234 | 39.62 | 0.02 | 43.83 | 0.07 | 0.23 | 16.07 | 0.19 | 100.02 | 82.82 | 1,677 |
| 15 | 257 | 39.54 | 0.01 | 43.27 | 0.04 | 0.23 | 16.06 | 0.23 | 99.37 | 82.61 | 1,783 |
| 14 | 271 | 39.72 | 0.03 | 44.17 | 0.09 | 0.23 | 15.41 | 0.22 | 99.87 | 83.54 | 1,715 |
| 13 | 291 | 39.68 | 0.01 | 43.97 | 0.09 | 0.21 | 15.73 | 0.24 | 99.93 | 83.19 | 1,852 |
| Drill core II14-83 | | | | | | | | | | | |
| 5 | 435 | 39.86 | 0.02 | 43.32 | 0.17 | 0.23 | 15.93 | 0.23 | 99.77 | 82.91 | 1,824 |
| 10 | 493 | 39.44 | 0.02 | 43.68 | 0.10 | 0.23 | 16.83 | 0.23 | 100.53 | 82.11 | 1,827 |
| 11 | 519 | 39.53 | 0.02 | 43.45 | 0.09 | 0.25 | 16.57 | 0.23 | 100.15 | 82.25 | 1,778 |
| 12 | 528 | 39.56 | 0.01 | 44.49 | 0.07 | 0.23 | 16.05 | 0.25 | 100.67 | 83.05 | 1,988 |
| 13 | 551 | 39.98 | 0.01 | 44.32 | 0.03 | 0.21 | 16.40 | 0.28 | 101.24 | 82.66 | 2,211 |
| 14 | 559 | 39.89 | 0.02 | 44.73 | 0.11 | 0.18 | 14.74 | 0.23 | 99.89 | 84.37 | 1,833 |
| 15 | 569 | 40.17 | 0.01 | 45.21 | 0.06 | 0.19 | 14.02 | 0.24 | 99.90 | 85.08 | 1,853 |
| 16 | 573 | 39.66 | 0.02 | 44.25 | 0.08 | 0.21 | 15.71 | 0.23 | 100.15 | 83.30 | 1,828 |
| 17 | 589 | 40.27 | 0.02 | 45.78 | 0.08 | 0.19 | 14.83 | 0.23 | 101.40 | 84.53 | 1,828 |
| 18 | 598 | 39.94 | 0.01 | 44.50 | 0.13 | 0.20 | 15.03 | 0.27 | 100.08 | 84.04 | 2,125 |
| 19 | 610 | 39.83 | 0.01 | 44.41 | 0.12 | 0.23 | 15.17 | 0.27 | 100.04 | 83.86 | 2,093 |
| 20 | 620 | 39.98 | 0.02 | 44.71 | 0.14 | 0.23 | 14.89 | 0.27 | 100.24 | 84.22 | 2,123 |
| 22 | 644 | 40.15 | 0.01 | 45.13 | 0.21 | 0.19 | 15.07 | 0.29 | 101.06 | 84.30 | 2,247 |
| 23 | 656 | 39.74 | 0.02 | 44.37 | 0.20 | 0.22 | 15.37 | 0.29 | 100.21 | 83.77 | 2,247 |
| 24 | 668 | 39.79 | 0.01 | 44.72 | 0.16 | 0.19 | 15.00 | 0.28 | 100.14 | 84.16 | 2,173 |
| 25 | 681 | 39.83 | 0.02 | 44.50 | 0.14 | 0.21 | 14.98 | 0.31 | 99.98 | 84.09 | 2,433 |
| 26 | 702 | 39.86 | 0.01 | 44.29 | 0.10 | 0.18 | 15.11 | 0.32 | 99.87 | 83.89 | 2,485 |
| 28 | 722 | 39.77 | 0.01 | 44.40 | 0.05 | 0.21 | 15.06 | 0.29 | 99.79 | 83.88 | 2,300 |
| 30 | 751 | 39.91 | 0.01 | 43.95 | 0.16 | 0.23 | 14.94 | 0.29 | 99.49 | 83.96 | 2,309 |
| 31 | 770 | 39.81 | 0.02 | 43.85 | 0.10 | 0.22 | 15.69 | 0.27 | 99.95 | 83.21 | 2,120 |
| 34 | 790 | 39.65 | 0.01 | 44.03 | 0.08 | 0.23 | 15.64 | 0.27 | 99.92 | 83.28 | 2,112 |
| 37 | 817 | 39.53 | 0.03 | 43.03 | 0.03 | 0.21 | 16.35 | 0.28 | 99.46 | 82.28 | 2,212 |
| Drill core II48-136 | | | | | | | | | | | |
| 1 | 93 | 39.64 | 0.01 | 44.76 | 0.08 | 0.21 | 15.53 | 0.23 | 100.45 | 83.61 | 1,780 |
| 2 | 107 | 39.86 | 0.01 | 44.58 | 0.07 | 0.21 | 15.07 | 0.26 | 100.06 | 83.96 | 2,045 |
| 4 | 124 | 39.98 | 0.01 | 44.98 | 0.09 | 0.21 | 14.62 | 0.24 | 100.13 | 84.50 | 1,881 |
| 6 | 146 | 39.52 | 0.03 | 45.29 | 0.04 | 0.23 | 15.07 | 0.25 | 100.42 | 84.10 | 1,961 |
| 8 | 158 | 39.74 | 0.01 | 44.79 | 0.08 | 0.23 | 14.91 | 0.24 | 99.99 | 84.15 | 1,875 |
| 9 | 174 | 39.83 | 0.02 | 44.54 | 0.05 | 0.22 | 15.42 | 0.23 | 100.30 | 83.60 | 1,787 |
| 10 | 188 | 39.99 | 0.04 | 43.91 | 0.11 | 0.22 | 15.89 | 0.23 | 100.40 | 83.05 | 1,835 |
| 11 | 193 | 40.06 | 0.00 | 44.87 | 0.08 | 0.21 | 15.12 | 0.23 | 100.58 | 84.01 | 1,835 |
| 12 | 205 | 39.74 | 0.02 | 44.36 | 0.05 | 0.23 | 15.54 | 0.22 | 100.16 | 83.44 | 1,729 |
| 13 | 218 | 39.42 | 0.01 | 44.24 | 0.10 | 0.21 | 15.78 | 0.24 | 100.01 | 83.25 | 1,890 |
| 14 | 231 | 39.43 | 0.00 | 44.05 | 0.12 | 0.22 | 16.14 | 0.24 | 100.19 | 82.89 | 1,850 |
| 15 | 238 | 40.01 | 0.05 | 44.21 | 0.09 | 0.22 | 15.52 | 0.24 | 100.34 | 83.44 | 1,880 |
| 16 | 241 | 39.62 | 0.02 | 43.78 | 0.11 | 0.24 | 15.89 | 0.24 | 99.89 | 82.99 | 1,884 |
| 17 | 252 | 39.92 | 0.05 | 44.31 | 0.10 | 0.24 | 15.54 | 0.24 | 100.39 | 83.46 | 1,873 |
| 18 | 255 | 39.57 | 0.02 | 43.86 | 0.11 | 0.27 | 16.03 | 0.23 | 100.10 | 82.90 | 1,845 |
| 21 | 286 | 38.99 | 0.04 | 44.18 | 0.08 | 0.20 | 16.00 | 0.24 | 99.73 | 83.03 | 1,901 |
| 22 | 294 | 39.92 | 0.05 | 43.57 | 0.16 | 0.21 | 16.38 | 0.24 | 100.53 | 82.57 | 1,854 |
| 28 | 343 | 39.39 | 0.02 | 43.99 | 0.03 | 0.23 | 16.00 | 0.24 | 99.88 | 82.88 | 1,847 |
| 29 | 351 | 39.92 | 0.02 | 44.76 | 0.12 | 0.21 | 15.06 | 0.26 | 100.34 | 84.08 | 2,037 |
| 30 | 357 | 39.78 | 0.03 | 45.29 | 0.11 | 0.20 | 14.45 | 0.26 | 100.11 | 84.77 | 2,049 |
| 33 | 410 | 39.54 | 0.01 | 44.97 | 0.10 | 0.21 | 14.90 | 0.29 | 100.03 | 84.25 | 2,302 |
| 34 | 430 | 39.42 | 0.01 | 44.88 | 0.06 | 0.20 | 14.26 | 0.27 | 99.10 | 84.75 | 2,103 |
| 35 | 442 | 39.67 | 0.03 | 45.32 | 0.10 | 0.20 | 14.44 | 0.29 | 100.06 | 84.78 | 2,285 |

**Table 1** (Contd.)

| Sample no. | Depth | $SiO_2$ | $Cr_2O_3$ | MgO | CaO | MnO | FeO | NiO | Total | Fo | Ni |
|---|---|---|---|---|---|---|---|---|---|---|---|
| | | (wt%) | | | | | | | | (mol%) | (ppm) |
| 36 | 450 | 39.73 | 0.02 | 44.90 | 0.07 | 0.21 | 14.96 | 0.31 | 100.21 | 84.14 | 2,468 |
| 38 | 465 | 39.26 | 0.01 | 44.77 | 0.12 | 0.21 | 14.93 | 0.29 | 99.60 | 84.18 | 2,282 |
| 39 | 473 | 39.70 | 0.02 | 44.62 | 0.06 | 0.20 | 14.53 | 0.22 | 99.36 | 84.45 | 1,766 |
| 40 | 476 | 40.08 | 0.02 | 45.43 | 0.06 | 0.19 | 14.40 | 0.20 | 100.39 | 84.79 | 1,608 |
| 41 | 486 | 39.67 | 0.06 | 44.96 | 0.02 | 0.20 | 15.16 | 0.26 | 100.34 | 83.93 | 2,036 |
| 43 | 505 | 39.54 | 0.01 | 44.72 | 0.07 | 0.21 | 15.20 | 0.27 | 100.02 | 83.88 | 2,083 |
| 44 | 516 | 39.57 | 0.01 | 44.91 | 0.06 | 0.21 | 15.06 | 0.23 | 100.05 | 84.05 | 1,789 |
| 47 | 548 | 39.33 | 0.03 | 44.13 | 0.13 | 0.20 | 15.25 | 0.23 | 99.30 | 83.73 | 1,835 |
| 51 | 568 | 39.68 | 0.02 | 44.60 | 0.15 | 0.19 | 14.86 | 0.19 | 99.69 | 84.25 | 1,515 |
| 53 | 577 | 39.25 | 0.02 | 43.77 | 0.07 | 0.23 | 15.36 | 0.20 | 98.90 | 83.40 | 1,578 |
| 58 | 599 | 38.73 | 0.03 | 44.49 | 0.09 | 0.25 | 15.98 | 0.21 | 99.77 | 83.11 | 1,657 |
| 62 | 623 | 39.52 | 0.02 | 44.08 | 0.11 | 0.22 | 15.96 | 0.23 | 100.14 | 83.04 | 1,820 |
| 63 | 630 | 39.65 | 0.02 | 43.29 | 0.15 | 0.23 | 16.21 | 0.24 | 99.79 | 82.60 | 1,878 |

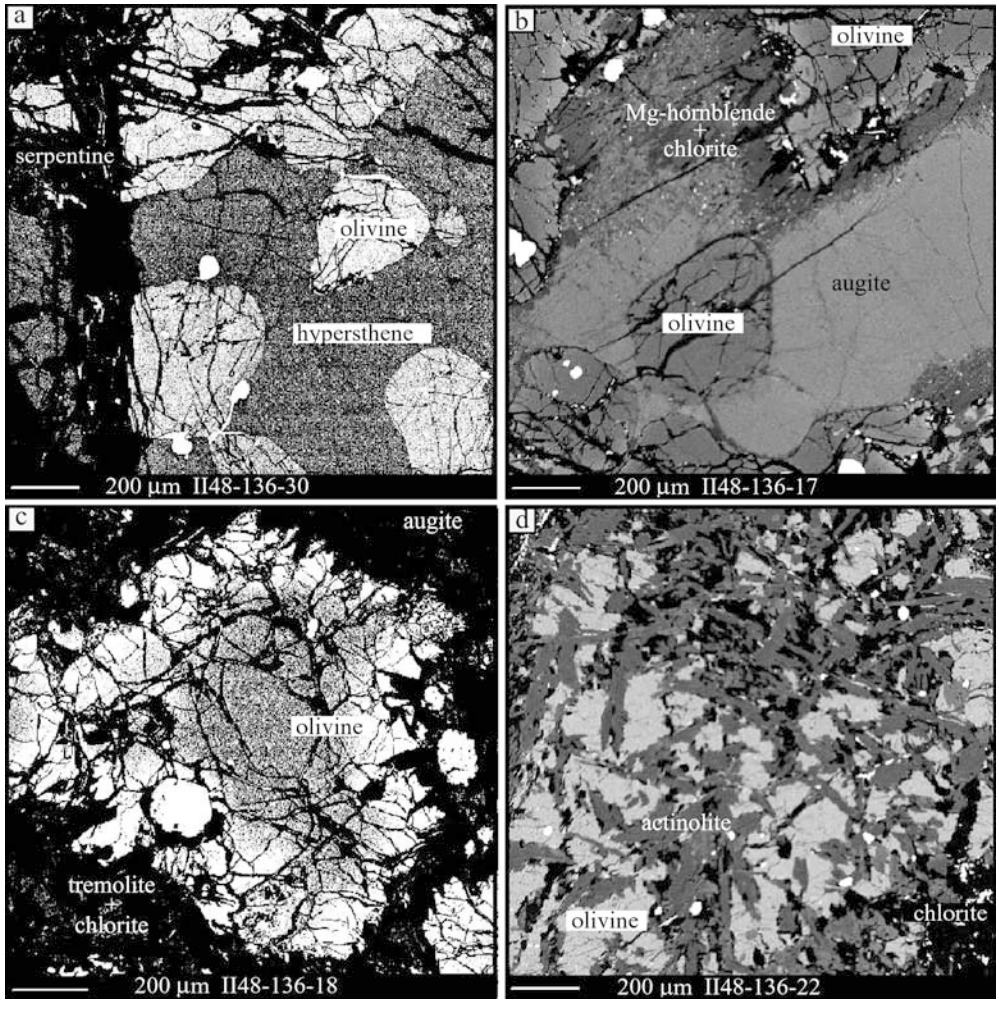


**Fig. 2a–d** Back-scattered electron images of olivine from the Jinchuan body. **a** Primary olivine occurs as inclusions in poikilitic hypersthene. **b** The rim of olivine in direct contact with secondary Mg-hornblende and chlorite recrystallized to form a more Fe-rich variant (brighter BSE image). **c** The size of the recrystallized rim of olivine increases in the samples with significant chlorite and tremolite alteration. **d** Intergrowth of actinolite with completely recrystallized olivine is present in highly altered samples

increases (Fig. 2c). At the most advanced stage of alteration, a characteristic mosaic texture is developed as a result of intergrowths of randomly oriented actinolite needles with completely recrystallized, Fe-rich olivine (Fig. 2d).

Figure 3a compares the compositions of recrystallized olivine associated with actinolite alteration with primary olivine from the same sample. The recrystallized olivine contains Fo and Ni up to 8 mol% and 500 ppm lower than primary olivine, respectively. In contrast, the effect of serpentinization on olivine compositions appears to be more subtle. As illustrated in Fig. 3b, the Fo and Ni contents of remnant olivine kernels and unaltered crystals from the same sample overlap.

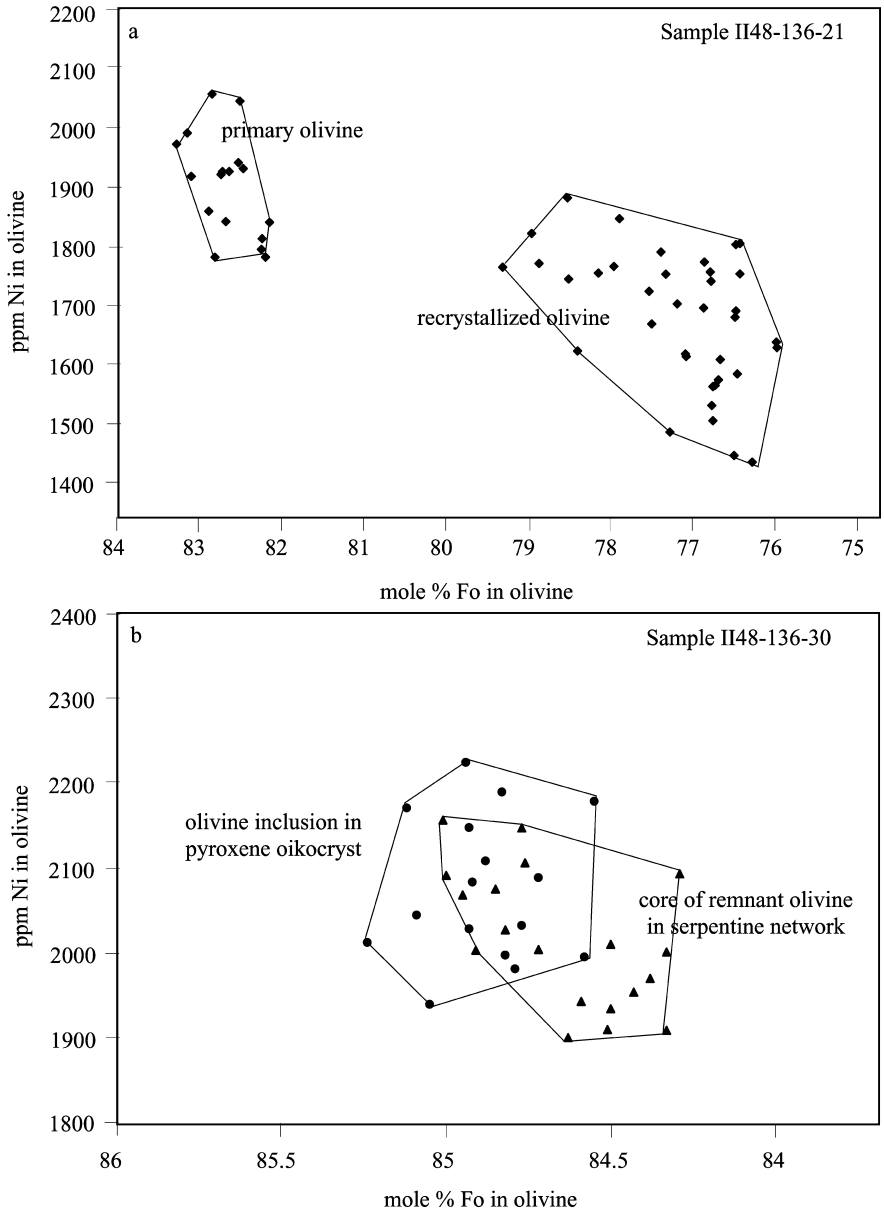


**Fig. 3** Compositional variations of different types of olivine from the Jinchuan body

In the following sections, we focus on the compositions of primary olivine. The compositions of recrystallized olivine associated with amphibole–chlorite alteration are excluded. As will become evident, there are slight compositional variations in primary olivine from a single sample. Such variability is a characteristic of the rocks and is documented. In the figures that follow, the compositions of individual grains instead of the average values of different grains from a single sample, are used.

## Downhole profiles of olivine compositions

In the following sections, we use the proportions of cumulus olivine and interstitial silicate and sulfide liquids in the samples, which were determined by De Waal et al. (2003), to assist our interpretation of olivine data.

Figure 4 illustrates downhole olivine distribution in drill core I14–16 that is located in the western segment of the Jinchuan body. The contents of olivine in the samples from this core vary between 50 and 82%. Interstitial silicate and sulfide liquids appear to compensate each other in the sulfide-bearing interval located close to the lower contact. There is no primary olivine preserved in the mineralized samples. In the sulfide-poor samples ($< 0.5$ wt% total sulfide) from the upper part of this drill core, the contents of Fo and Ni in olivine from a single sample vary up to 2 mol% and 200 ppm, respectively. There are two notable downhole discontinuities of olivine Fo compositions in the sulfide-poor interval. Accordingly, this interval is subdivided into three zones. The central zone (zone 2) is characterized by olivine with

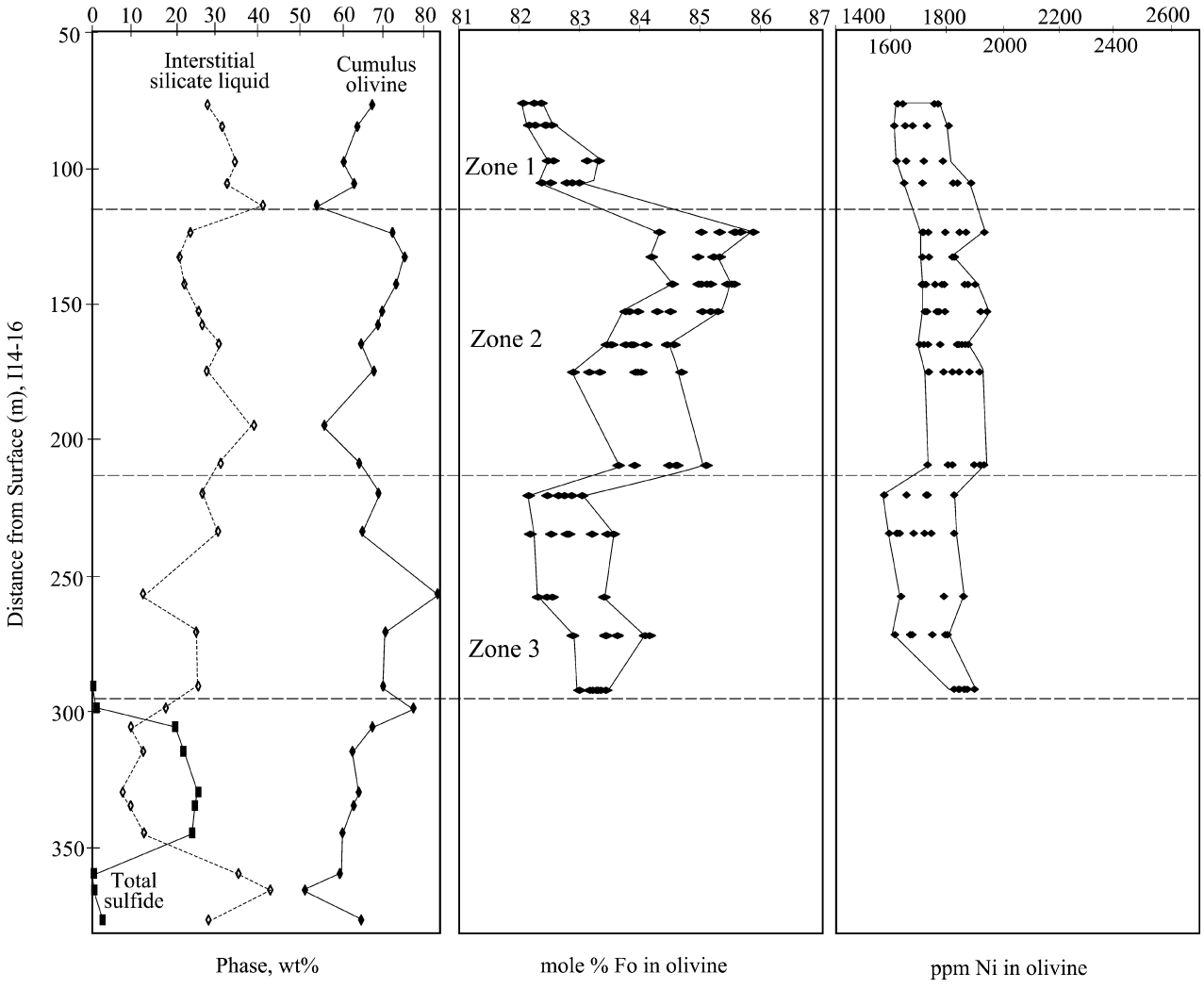


**Fig. 4** Compositional variations of olivine in borehole I14-16 located in the western segment of the Jinchuan body

relatively high Fo contents (83–86 mol%) as compared to the other zones. The Fo contents of olivine in the lower and upper units (zones 1 and 3, respectively) are up to 2.5 mol% lower. The contents of Ni in olivine are rather similar throughout the entire interval (1,600–1,800 ppm).

Figure 5 illustrates the compositional variations of olivine from drill core II14–83 in the central segment. This drill core intercepted ore body #1. Similar to the previous drill core, the contents of interstitial silicate liquid and total sulfide in the rocks appear to compensate each other. The contents of cumulus olivine in the samples from this core vary between 40 and 75%. Variations in Fo contents of different olivine grains from a single sample are similar for both mineralized and unmineralized intervals, ranging between 1 and 2 mol%. Variations in Ni contents of different olivine grains from a single sample from the mineralized interval are between 200 and 400 ppm. Variations in Ni contents of different olivine grains from a single sample from the unmineralized interval are slightly lower, ranging between 150 and 300 ppm.

The unmineralized interval in II14–83 (Fig. 5) is characterized by olivine with Fo contents ranging between 82 and 84 mol%. Olivine with slightly higher Fo content (up to 86 mol%) occurs in the middle part of the mineralized interval. The mineralized interval may be further divided into three zones. The lower zone is characterized by relatively low Fo and intermediate Ni contents in olivine. The central zone is characterized by higher Fo and Ni contents in olivine. The upper zone is characterized by large variations in both Fo and Ni contents in olivine. The average compositions of sulfide (recalculated to 100% sulfide, for details see De Waal et al. 2003) in different zones are different. The sulfide in the central zones has the highest Ni content (9.3 wt%). The Ni contents of sulfide in the lower and upper zones are notably lower, ranging from 8.7 to 6.5 wt%, respectively.

Figure 6 illustrates the compositional variations of olivine in drill core II48–136 from the eastern segment. This drill core intercepted about 300 m of mineralized rocks in the lower part and about 400 m of

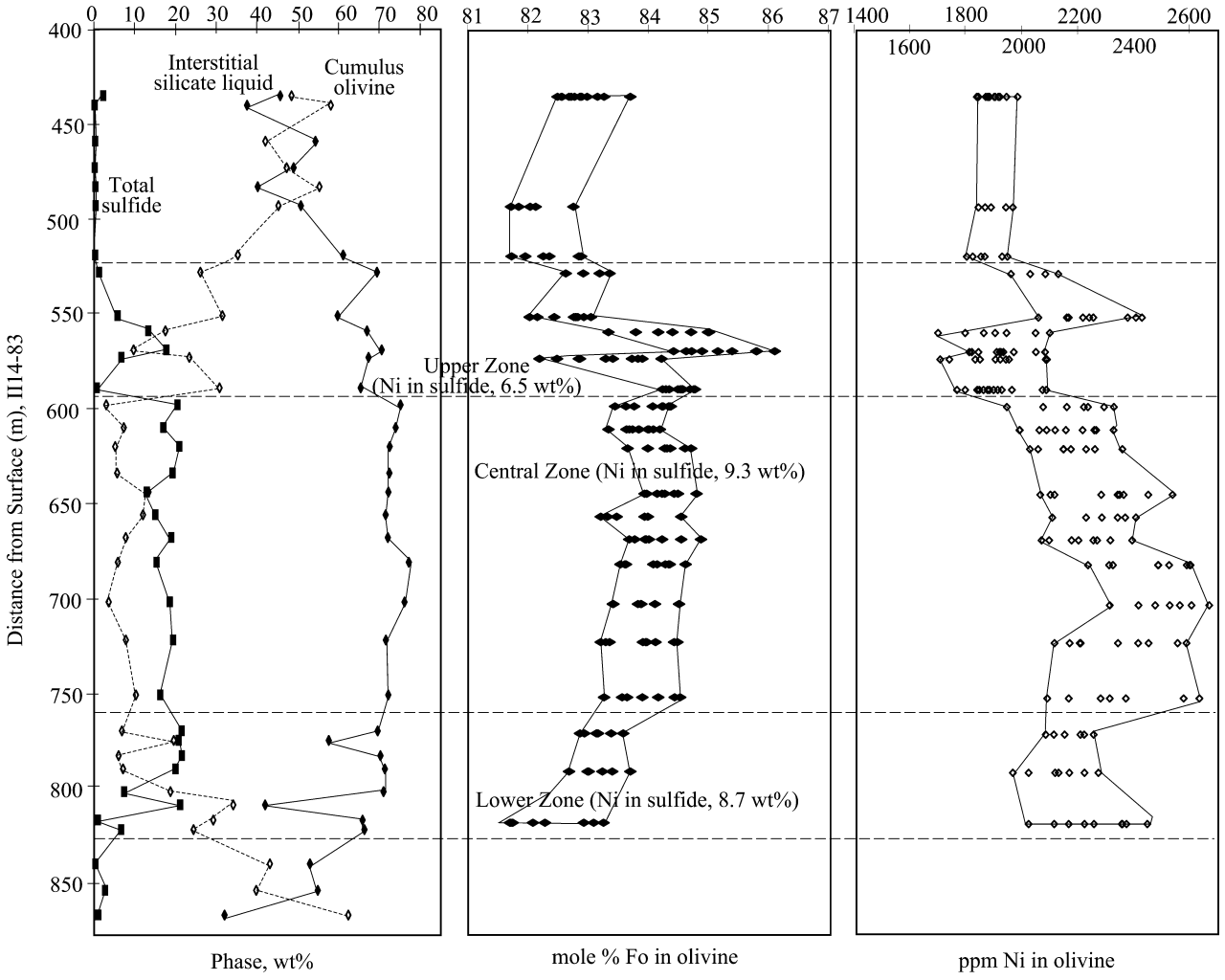


**Fig. 5** Compositional variations of olivine in borehole II14–83 located in the central segment of the Jinchuan body

unmineralized rocks in the upper part. The contents of sulfide in the samples from this core are compensated by the contents of olivine as well as interstitial silicate liquid. The contents of olivine in the samples vary between 40 and 80%. Variations in Fo and Ni contents of different olivine grains from a single sample are similar for both mineralized and unmineralized intervals, averaging near 1.5 mol% and less than 300 ppm, respectively. The mineralized interval may be further divided into three zones. The contents of Ni in olivine increase from the lower zone through the central zone to the upper zone. The content of Ni in sulfide also increases upward (5.6, 6.4, and 11.2 wt% in the Lower, Central, and Upper Zones, respectively).

## Modeling

The most likely influences on the compositions of magmatic olivine are parental magma composition, fractional crystallization and sub-solidus reaction with interstitial silicate and sulfide liquids.

The compositions of early cumulus olivine may be modified by re-equilibration with trapped silicate liquid. Olivine that crystallizes from the trapped silicate liquid will be poorer in Fo and Ni contents than the early-formed cumulus olivine. Barnes (1986) referred to this effect as a "trapped liquid shift".

In the presence of a sulfide liquid, Ni and Fe will exchange between olivine and sulfide liquid according to the reaction:

$$NiO^{olivine}+FeS^{sulfide}= NiS^{sulfide}+FeO^{olivine}. \quad (1)$$

The exchange partition coefficient $K_D$ for this reaction is defined as:

$$K_D= (NiS/FeS)^{sulfide}/(NiO/FeO)^{olivine}, \quad (2)$$

where concentrations are expressed in mole fractions. $K_D$ is related to the equilibrium constant, K, by the expression:

$$K = K_D(\gamma_{NiS}/\gamma_{FeS})^{sulfide}/(\gamma_{NiO}/\gamma_{FeO})^{olivine}, \quad (3)$$

where $\gamma$ refers to the activity coefficient.

The experiments of Brenan (2003) indicate that $K_D$ varies between 5 and 35, depending on temperature,

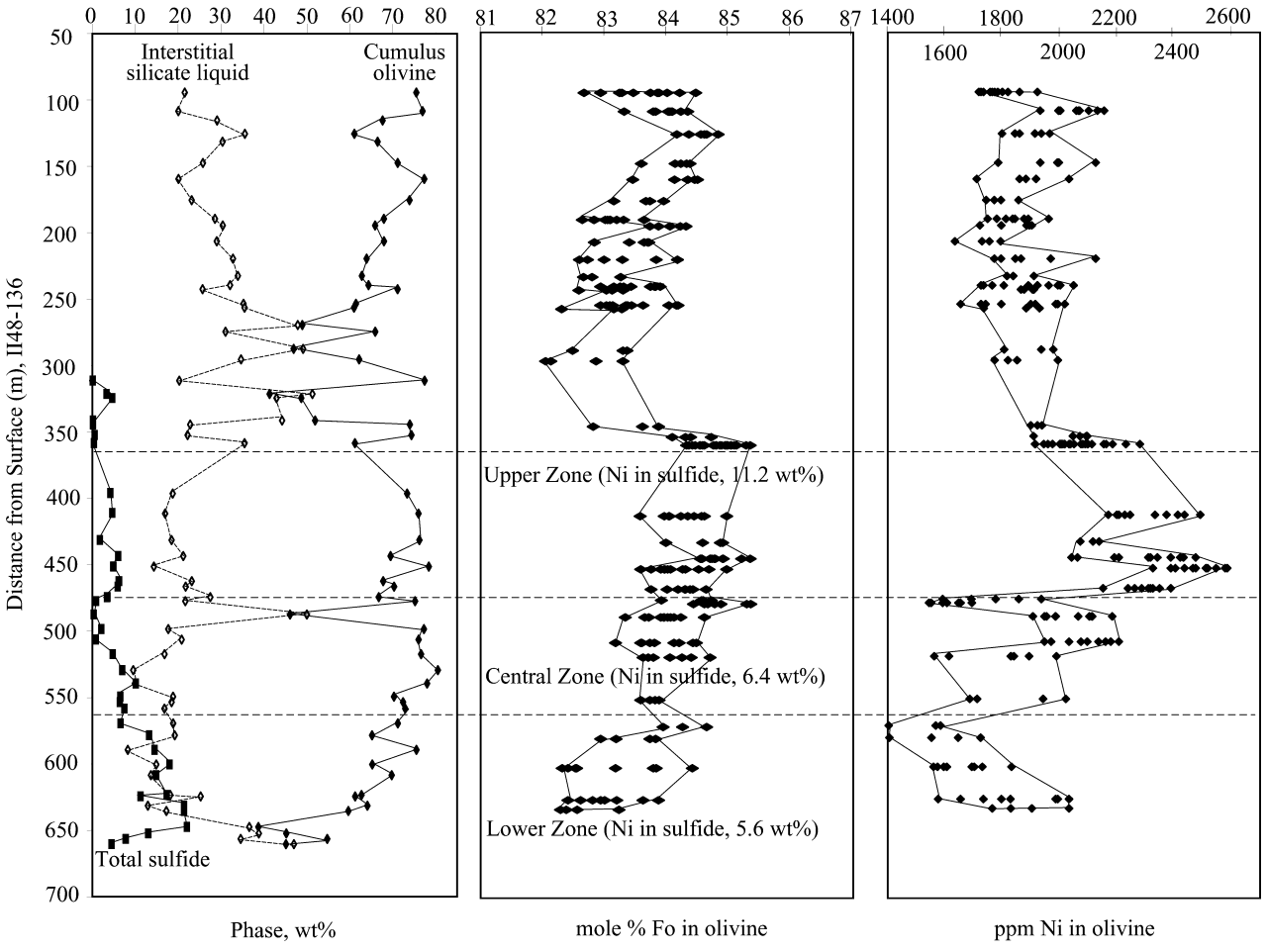


**Fig. 6** Compositional variations of olivine in borehole II48–136 located in the eastern segment of the Jinchuan body

$f_{S2}$, $f_{O2}$, and the content of Ni in the sulfide liquid. The value of $K_D$ will remain constant in a closed system in which the content of Ni in the sulfide liquid and other intrinsic variables are constant. In such a system, the Fe–Ni exchange reaction will produce a negative Fo–Ni relationship in olivine. Examples of such a relationship in some magmatic sulfide deposits have been given by Barnes and Naldrett (1985) and Li et al. (2001a, 2003a).

## Sulfide-poor samples

The compositions of olivine in sulfide-poor samples from different parts of the Jinchuan body are compared in Fig. 7. The model curves illustrate the compositions of olivine crystallizing from a parental magma with 330 ppm Ni, 11.5 wt% MgO, and 11.2 wt% FeO. The FeO and MgO compositions are from Chai and Naldrett (1992a). Fractional crystallization of olivine from the magma is simulated using a Mg–Fe exchange coefficient $K_D$, or $(FeO/MgO)^{olivine}/(FeO/MgO)^{magma} = 0.3$ (Roeder and Emslie 1970) and an olivine–magma Ni partition coefficient, or $D^{Ni} = 7$. The $D^{Ni}$ value used in the calculations is within the range of values from submarine basalts (Li et al. 2003b).

The shifts in olivine compositions shown in Fig. 7 are due to trapped silicate liquid crystallization. They have been determined using mass balance calculations and the abundance and compositions of cumulus and intercumulus olivine in the samples. The compositions of intercumulus olivine are calculated assuming that the trapped silicate liquid crystallized equal amounts of olivine, clinopyroxene, and plagioclase. The distributions of Ni among the silicate minerals are calculated assuming that $D^{Ni}$ values for olivine, clinopyroxene, and plagioclase are 7, 1, and 0, respectively.

The results of our calculations indicate that less than 5% fractional crystallization of olivine from the magma, followed by re-equilibration of the olivine with up to 30% of trapped silicate liquid, adequately accounts for the compositions of olivine from all sulfide-poor samples except those from zone 2 of I14–16 (Fig. 7). Variations of Fo content (~3 mol%) in olivine from zone 2 of I14–16 are also within the range produced by local equilibration of the olivine with up to 30% of trapped silicate liquid. But the content of Ni in olivine from this zone remains rather constant instead of decreasing with Fo content, which may have resulted from partial equili-

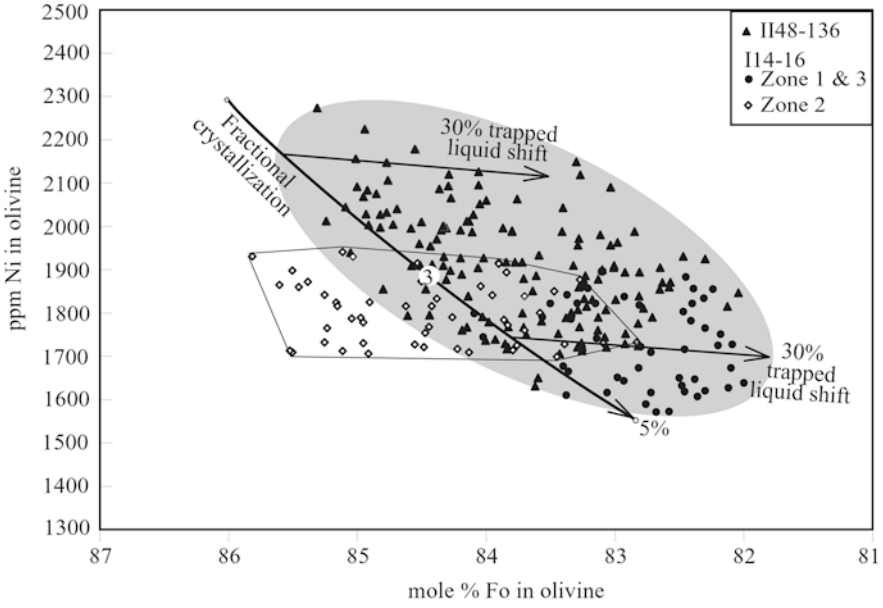


**Fig. 7** Modeling of olivine fractional crystallization and re-equilibration of the olivine with interstitial silicate liquids. The model curve, *a* represents initial magma with 11.2 wt% FeO, 11.5 wt% MgO (Chai and Naldrett 1992a) and 330 ppm Ni. Olivine fractional crystallization is simulated assuming olivine-magma $D^{Ni} = 7$ and $(FeO/MgO)^{olivine}/(FeO/MgO)^{magma} = 0.3$. The shifts in olivine compositions are due to the effect of trapped silicate liquid crystallization. They are determined using mass balance calculations and the abundances and compositions of cumulus and intercumulus olivine in the samples. The compositions of intercumulus olivine are calculated assuming that the trapped silicate liquid crystallized equal amounts of olivine, clinopyroxene, and plagioclase. The distributions of Ni among the silicate minerals are calculated assuming that $D^{Ni}$ values for olivine, clinopyroxene, and plagioclase are 7, 1, and 0, respectively

bration of the olivine with a sulfide liquid. But this does not seem to be consistent with low sulfide contents in the samples. One possibility is that a sulfide liquid was present during the crystallization of olivine from interstitial silicate liquid and the sulfide liquid was subsequently removed from the rocks.

## Sulfide-bearing samples

The compositions of olivine in sulfide-bearing samples from different parts of the intrusion are compared in Fig. 8. Variations of Fo content in olivine from each zone are $< 4$ mol%, which are consistent with local equilibration of the olivine with up to 30% of trapped magma. The negative Fo–Ni relationship of olivine from each zone is apparently related to local equilibration of the olivine with trapped sulfide liquids. Reactions of olivine with trapped silicate and sulfide liquids may have taken place simultaneously on cooling. But the final compositions of olivine record the results of olivine-sulfide Fe–Ni exchange reaction because the final crystallization temperature of a sulfide liquid is much lower than that of a silicate liquid of basaltic composition (i.e., ~850 versus ~1,050 °C).

The compositional variations of olivine from the sulfide-bearing samples indicate that multiple sulfide liquids of different Ni contents were involved at Jinchuan. This is consistent with whole-rock chemical data from De Waal et al. (2003). The weighted average contents of Ni in the sulfide fractions (recalculated to 100% sulfide from whole-rock analyses of De Waal et al. 2003) in the lower, central, and upper zones of ore body #2 intercepted by II48–136 are 5.6, 6.4, and 11.2 wt%, respectively. The contents of Ni in the sulfide liquids calculated from olivine compositions increase from ~7.5 wt% in the lower zone, through ~8.5 wt% in the central zone, to ~10 wt% in the upper zone (Fig. 8a). The absolute values differ, but the zoning pattern across the ore body indicated by actual analyses and modeled results are consistent.

The weighted average contents of Ni in the sulfide fractions in the lower, central and upper zones of ore body #1 intercepted by II14–83 are 8.7, 9.3, and 6.5 wt%, respectively (data from De Waal et al. 2003). The Ni contents of the sulfide liquids calculated from olivine compositions increase from ~8.5 wt% in the lower and upper zones to 10 wt% in the central zone (Fig. 8b). Although the absolute values differ, the zoning pattern across the ore body indicated by actual analyses and modeled results are consistent, as observed in ore body #2.

There are some uncertainties associated with the modeled results. These include local compositional variations due to fractional crystallization of a sulfide liquid on cooling and local redistributions of Ni during hydrothermal alteration. Fractional crystallization of a monosulfide solid solution from a sulfide liquid may change Ni/Cu ratio in the residual liquid as a result of different crystal–liquid partition coefficients for Ni and Cu (Li et al. 1996). The metal zonation in the Strathcona Ni–Cu sulfide deposit at Sudbury, Canada, is thought to result from this process (Keays and Crocket 1970; Li

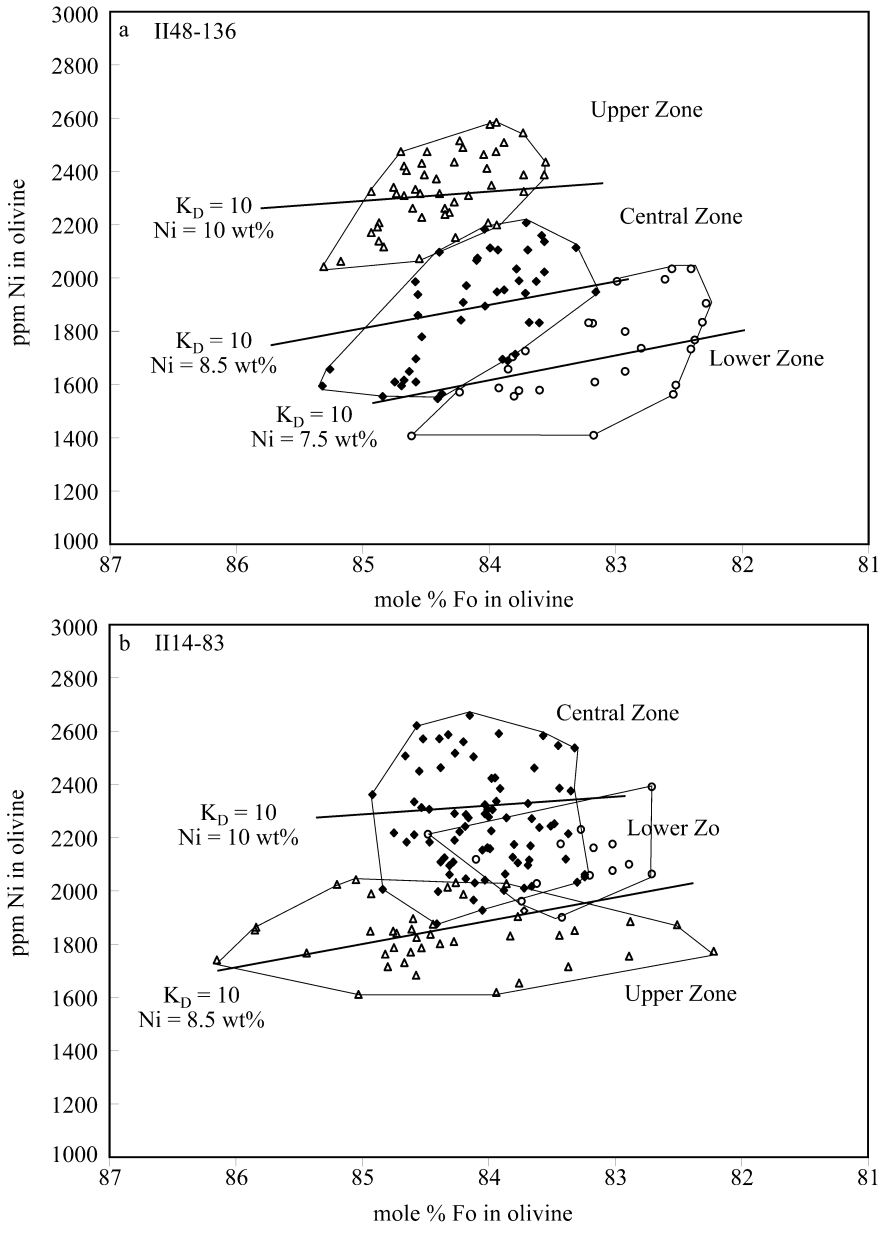


**Fig. 8** Modeling of compositional variations in olivine and coexisting sulfide liquids as a result of Fe–Ni exchange between the two phases. Assuming that the mole ratio of $(NiS/FeS)^{sulfide}/(NiO/FeO)^{olivine}$, or $K_D$, equals to 10, our calculations indicate that the Ni contents in the original sulfide liquids in the three different ore zones in the eastern segment (drill core II48–136) increased from about 7.5 wt% in the lower zone through to ~8.5 wt% in the central zone to ~10 wt% in the upper zone. Similarly, the calculated Ni contents in the original sulfide liquids in the center segment (drill core II14–83) increased from about 8.5 wt% in the lower and upper zones to 10 wt% in the central zone. These trends are consistent with the results of whole rock analyses from De Waal et al. (2003)

et al. 1992). This process, however, is not important at large scale (e.g., a few meters in distance) unless there are some preexisting structures (e.g., the footwall breccias at Sudbury) that may permit the fractionated liquids to escape. Examples of Ni redistribution between sulfides and silicates have been reported for disseminated sulfide ores associated with antigorite–carbonate alteration in the Mt. Keith komatiite-hosted Ni deposit in western Australia (Barnes and Hill 2000) and for weakly sulfide-mineralized rocks with actinolite alteration in the Sääksjärvi mafic–ultramafic complex in southern Finland (Mancini and Papunen 2000). This redistribution process, however, is unlikely to be significant for sulfide-rich rocks (e.g., sulfide > 5 wt%).

Data from Chai and Naldrett (1992a) indicate that the concentric enrichment of Ni, as observed in ore body #1, is also present in ore body #24. Chai and Naldrett (1992a) also observed concentric enrichment of PGE in these two ore bodies and vertical enrichment of PGE in ore body #2. In addition, they found that the average contents of PGE in ore body #2 are about one order lower than that in both ore bodies #1 and #24 (e.g., ~1 versus ~10 ppm Pt).

## Discussion

Petrographgic data indicate that the Jinchuan rock samples represent mixtures of cumulus olivine and interstitial silicates and/or sulfides. Using the modeled parental magma of Chai and Naldrett (1992a), the average compositions of cumulus olivine and whole-rock compositions corrected for the presence of Cr-spinel, $H_2O$, and $CO_2$, De Waal et al. (2003) calculated the

modal concentrations of olivine in individual samples by least squares optimization. Their results indicate that the Jinchuan rock samples contain cumulus olivine varying between 40 and 80 wt%, similar to observations in thin sections.

The results of our calculations presented above indicate that a maximum of 5% crystallization of olivine from the parental magma adequately describes the compositions of cumulus olivine in the intrusion. The magma/olivine ratio in such a system is thus more than 19. Mass balance calculations using these two constraints indicate that the current Jinchuan body accounts for less than 2% of the total parental magma.

Significant magma missing at Jinchuan is also indicated by high sulfide contents in the rocks. The average sulfide content in the Jinchuan body is about 5 wt%. Using the magma compositions of Chai and Naldrett (1992a), a liquidus temperature and $FeO/Fe_2O_3$ ratio that are calculated using the silicate liquid model MELTS of Ghiorso and Sack (1995), and the sulfur solubility equation of Li et al. (2001b), the solubility of sulfur in the Jinchuan magma is estimated to be ~1,150 ppm (~0.3 wt% FeS) under an assumed total pressure of 3 Kb and an oxidation state equivalent to the quartz–fayalite–magnetite buffer. Assuming that the amount of the trapped magma in the Jinchuan rocks is 50 wt%, which is the higher end of the values determined by De Waal et al. (2002), mass balance calculations indicate that the magma now represented by the Jinchuan body only accounts for about 3% of the total magma in which the total sulfide in the body could have been dissolved. Another 97% of the total mass of the parental magma is not accounted for by the current Jinchuan body, similar to the conclusion based on the average content of cumulus olivine in the rocks.

Although the volume of missing magma at Jinchuan has never been quantitatively assessed previously, the mass balance problem in general has been known to many previous investigators such as Tang and co-workers (Tang 1990, 1993; Tang and Li 1995), and Chai and Naldrett (1992a), and these two groups have proposed competing models to address this issue.

Tang and co-workers (Tang 1990, 1993; Tang and Li 1995) proposed that the Jinchuan deposit was formed by injection of sulfide magma into a linear structure at Jinchuan and the missing magma intruded elsewhere. In this model, the magma and sulfide liquid were separated by density-induced liquid stratification in a staging magma chamber, and the sulfide-bearing magma and pure sulfide liquid were sequentially squeezed into the Jinchuan structure.

Chai and Naldrett (1992a) proposed that the Jinchuan intrusion represents the root of a much larger layered intrusion and the missing magma formed the upper part of the intrusion that has been eroded. They proposed that the eastern segment represents the higher level of the intrusion. In this model, the concentric enrichments of metals in both ore bodies #1 and #24 are thought to result from interaction of early-formed sulfide liquid in the conduit with new surges of PGE-undepleted magma using the same conduit, and low PGE in ore body #2 is thought to result from further sulfide segregation after the magma reached the Jinchuan chamber. This late-stage sulfide liquid was poor in PGE because the magma became depleted in PGE after reacting with the sulfide liquids in the conduit.

Chai and Naldrett (1992a) argued that the sub-horizontal lithological layering in the eastern segment is evidence for gravitational settling of cumulus olivine and sulfide liquids in the floor of the Jinchuan chamber. The lithological layering in the Jinchuan body, as shown in some cross sections constructed in the 1970s by the Chinese exploration geologists, may be highly interpretative because that was the time when the concept of layered intrusions begun to flourish in China. The samples from this study do not indicate any systematic lithological layering in the sulfide-poor intervals in any of the segments.

Chai and Naldrett (1992a) suggested that sulfide saturation in the chamber overlying the eastern segment was caused by magma mixing. But Li et al. (2001c) and Cawthorn (2002) demonstrated that mixing of two S-undersaturated magmas does not induce sulfide saturation. Olivine fractional crystallization may eventually drive the residual magma to sulfide saturation. But the amount of immiscible sulfide liquid segregated during this process is small and would tend to be dispersed throughout the entire column of silicate cumulates. Furthermore, the sulfide liquids would become depleted in Ni and PGE with time. Gravitational settling of the sulfide liquids would produce a sulfide ore body with upward instead of downward metal depletion that is observed in ore body #2.

Low PGE in ore body #2 may have been due to a lack of metal upgrading in the sulfide by new magma, or the new surges of magma were already depleted in PGE due to a previous reaction with sulfide liquids in other parts of the conduit.

There is a consensus that initial sulfide saturation took place in a staging chamber because in situ sulfur addition and siliceous contamination that are critical to sulfide saturation in a basaltic magma (Li and Naldrett 1993; Ripley and Li 2003) are not found in the Jinchuan body (Chai and Naldrett 1992a; Tang and Li 1995). If initial sulfide segregation indeed took place in a staging chamber, metal upgrading by magma from the staging chamber is no longer important because the magma had already lost much of its PGE to the sulfide liquids in the staging chamber. Therefore, variations of PGE in different zones of a single ore body, as well as in different ore bodies, are more likely to result from multiple sulfide liquids from depth. Variable sulfide liquid compositions may have resulted from fractional segregation of the sulfide liquids in a staging chamber. The early-segregated sulfide liquids will contain more PGE than the late-segregated sulfide liquids because of the extremely high partition coefficients of PGE between a sulfide liquid and magma.

Tang and co-workers (Tang 1993; Tang and Li 1995) proposed that the parental magma of the Jinchuan body is of ultramafic composition and that the Jinchuan olivine-rich rocks are products of in situ crystallization of the ultramafic magma. In contrast, Chai and Naldrett (1992b) suggested that the Jinchuan parental magma is of basaltic composition and that high olivine contents in the Jinchuan rocks resulted from crystal sorting such as flow differentiation in the central segment and gravitational settling in the eastern segment. Our olivine data agree with the suggestion of Chai and Naldrett (1992b) that the parental magma of the Jinchuan body is of basaltic composition. De Waal et al. (2003) suggested that the magma may have carried >40% olivine and variable amounts of sulfide droplets upon emplacement at Jinchuan. They referred to this olivine- and sulfide-laden magma as "crystal mush".

## Conclusions

1. Olivine re-crystallization is found to be associated with actinolite alteration in the Jinchuan rocks.
2. Compositional variations of primary olivine from the sulfide-poor samples are adequately accounted for by a small degree of olivine crystallization (<5%) from a basaltic magma, followed by local re-equilibration of the olivine with up to 30% trapped silicate liquid.
3. In the sulfide-bearing samples, the compositions of primary olivine record the results of local olivine-sulfide Fe–Ni exchange that finished after trapped silicate liquid crystallized in the rocks.
4. Multiple sulfide liquids of different compositions, possibly formed by fractional segregation from a basaltic magma in a staging chamber, are involved in the formation of different ore zones.
5. High concentrations of cumulus olivine with limited compositions in the different parts of the Jinchuan body are more consistent with emplacement of olivine-laden, basaltic magma than in situ crystallization of olivine-free, ultramafic magma.
6. Sulfide enrichment toward the center in the central segment and toward the lower contact in the eastern and western segments may be in part related to flow differentiation and gravitational settling during magma ascent through the conduit, respectively.

**Acknowledgements** We thank Tong Zongli and Jinchuan NF Metals Ltd. for their assistance in field work. Comments from Steve Barnes and Finn Barrett on an earlier draft of this paper and reviews by Mei-Fu Zhou, Grant Cawthorn, and Associate Editor Peter Lightfoot are greatly appreciated. Financial support for this work was provided through a grant (EAR 0104580) from the National Science Foundation of the United States to C. Li and E.M. Ripley, through a postdoctoral fellowship from University of Pretoria to Z.H. Xu, and through a fund from the Center for Research on Magmatic Ore Deposits of the University of Pretoria to S.A. de Waal.

## References

Barnes SJ (1986) The effect of trapped liquid crystallization on cumulus mineral compositions in layered intrusions. Contrib Mineral Petrol 93:524–531

Barnes SJ, Hill RET (2000) Metamorphism of komatiite-hosted Ni sulfide deposits. In: Spry PG, Marshall B, Frank MV (eds) Metamorphosed and metamorphogenic ore deposits. Soc Econ Geol Rev Econ Geol 11:203–215

Barnes SJ, Naldrett AJ (1985) Geochemistry of the JM (Howland) Reef of the Stillwater Complex, Minneapolis Adit area, I. sulfide chemistry and sulfide–olivine equilibrium. Econ Geol 80:627–645

Barnes SJ, Tang ZL (1999) Chrome spinels from the Jinchuan Ni–Cu sulfide deposit, Gansu province, People's Republic of China. Econ Geol 94: 343–356

Brenan JM (2003) Effects of $f_{S2}$, $f_{O2}$, temperature, and melt composition on the Fe–Ni exchange between olivine and sulfide liquid: implications for natural olivine-sulfide assemblages. Geochim Cosmochim Acta 67:2663–2681

Cawthorn RG (2002) The role of magma mixing in the genesis of PGE mineralization in the Bushveld Complex: thermodynamic calculations and new interpretations: a discussion. Econ Geol 97:663–666

Chai G, Naldrett AJ (1992a) Characteristics of Ni–Cu–PGE mineralization and genesis of the Jinchuan deposit, northwest China. Econ Geol 47:1475–1495

Chai G, Naldrett AJ (1992b) The Jinchuan Ultramafic Intrusion: cumulate of a high-Mg basaltic magma. J Petrol 33:277–303

De Waal SA, Xu ZH, Li C, Mouri H (2003) Emplacement of dense, viscous crystal mushes, Jinchuan Ultramafic Intrusion, western China. Can Mineral (in press)

Ghiorso MS, Sack RO (1995) Chemical mass transfer in magmatic processes. IV. A revised and internally consistent thermodynamic model for the interpolation and extrapolation of liquid–solid equilibria in magmatic systems at elevated temperatures and pressures. Contrib Mineral Petrol 119:197–212

Keays RR, Crocket JH (1970) A study of precious metals in the Sudbury Ni irruptive ores. Econ Geol 65:438–450

Lesher CM, Keays RR (2002) Komatiite-associated Ni–Cu–(PGE) deposits: mineralogy, geochemistry, and genesis. In: Cabri LJ (ed) The geology, geochemistry, mineralogy, and mineral beneficiation of the platinum-group elements. Can Inst Mining Metall Petrol Spec Vol 54:579–617

Li C, Naldrett AJ (1993) Sulfide capacity of magma: a quantitative model and its application to the formation of the sulfide ores at Sudbury. Econ Geol 88:1253–1260

Li C, Barnes S-J, Mackovicky E (1996) Partitioning of Ni, Cu, Ir, Rh, Pt and Pd between monosulphide solid solution and sulphide liquid: effects of temperature and composition. Geochim Cosmochim Acta 60:1231–1238

Li C, Ripley EM, Naldrett AJ (2003a) Compositional variations of olivine and sulfur isotopes in the Noril'sk and Talnakh intrusions, Siberia: implications for ore forming processes in dynamic magma conduits. Econ Geol 98:69–86

Li C, Ripley EM, Mathez EA (2003b) The effect of S on the partitioning of Ni between olivine and silicate melt in MORB. Chem Geol 201:295–306

Li C, Naldrett AJ, Coats CJA, Johannessen P (1992) Platinum, palladium, gold, and copper-rich stringers at the Strathcona Mine, Sudbury: their enrichment by fractionation of a sulfide liquid. Econ Geol 87:1584–1598

Li C, Naldrett AJ, Ripley EM (2001a) Critical factors for the formation of a Ni–copper deposit in an evolved magmatic system: lessons from a comparison of the Pants Lake and Voisey's Bay sulfide occurrences in Labrador, Canada. Miner Deposita 36:85–92

Li C, Maier WD, de Waal SA (2001b) The role of magma mixing in the genesis of PGE mineralization in the Bushveld Complex: thermodynamic calculations and new interpretations. Econ Geol 96:653–662

Li C, Maier WD, de Waal SA (2001c) Magmatic Ni–Cu versus PGE deposits: contrasting genetic controls and exploration implication. South African J Geol 104:309–318

Lightfoot PC, Keays RR, Doherty W (2001) Chemical evolution and origin of Ni sulfide mineralization in the Sudbury Igneous Complex, Ontario, Canada. Econ Geol 96:1855–1876

Mancini F, Papunen H (2000) Metamorphism of Ni–Cu sulfides in mafic–ultramafic intrusions: the Svecofennian Sääksjärvi Complex, southern Finland. In: Spry PG, Marshall B, Frank MV (eds) Metamorphosed and metamorphogenic ore deposits. Soc Econ Geol Rev Econ Geol 11:217–231

Naldrett AJ (1998) World-class Ni–Cu–PGE deposits: key factors in their genesis. Miner Deposita 34:227–240

Naldrett AJ, Lightfoot PC (1999) Ni–Cu–PGE deposits of the Noril'sk region, Siberia: their formation in conduits for flood basalt volcanism. In: Keays RR, Lesher CM, Lightfoot PC, Farrow CFG (eds) Dynamic processes in magmatic ore deposits and their application to mineral exploration. Geol Assoc Can Short Course Notes XIII:195–250

Ripley EM, Li C (2003) Sulfur isotopic exchange and metal enrichment in the formation of magmatic Cu–Ni–(PGE) deposits. Econ Geol 98:635–641

Roeder PL, Emslie RF (1970) Olivine–liquid equilibrium. Contrib Mineral Petrol 29:275–289

Tang ZL (1990) Mineralization model of the Jinchuan sulfide Cu–Ni deposit (in Chinese). Modern Geol 4:55–64

Tang ZL (1993) Genetic models of the Jinchuan Ni–copper deposit. In: Kirkham RV, Sinclair WD, Thorpe RI, Duke JM (eds) Mineral deposit modeling. Geol Assoc Can Spec Pap 40:389–401

Tang ZL, Li WY (1995) The metallogenetic model and geological contrast on the Jinchuan platinum-bearing Ni–Cu sulfide deposit (in Chinese). Geological Publishing House, Beijing

Tang ZL, Yang J, Xu S, Tao X, Li W (1992) Sm–Nd dating of the Jinchuan ultramafic rock body, Gansu, China (in Chinese). Chin Sci Bull 37:1988–1991

Zhou M-F, Yang Z-X, Song X-Y, Keays RR, Lesher CM (2002) Magmatic Ni–Cu–(PGE) sulfide deposits in China. In: Cabri LJ (ed) The geology, geochemistry, mineralogy, and mineral beneficiation of the platinum-group elements. Can Inst Mining Metall Petrol Spec Vol 54:619–636